Science Advances
AAAS

advances.sciencemag.org/cgi/content/full/6/6/eaay4603/DC1

Supplementary Materials for

Tropical forests did not recover from the strong 2015–2016 El Niño event

Jean-Pierre Wigneron*, Lei Fan*, Philippe Ciais, Ana Bastos, Martin Brandt, Jérome Chave, Sassan Saatchi, Alessandro Baccini, Rasmus Fensholt

*Corresponding author. Email: jean-pierre.wigneron@inra.fr (J.-P.W.); fanlei20088@163.com (L.F.)

Published 5 February 2020, *Sci. Adv.* **6**, eaay4603 (2020)
DOI: 10.1126/sciadv.aay4603

This PDF file includes:

Fig. S1. Scatterplots between yearly mean L-VOD in 2011 and benchmark AGC density maps.
Fig. S2. Anomaly of the P – ET deficit (mm) superimposed on the anomalies of AGC stocks estimated from the L-VOD index in the tropics.
Fig. S3. Biome classes for 2001 to 2010 based on the MODIS IGBP products over the tropics.
Fig. S4. Anomalies of AGC stocks estimated from the L-VOD index in tropical regions.
Fig. S5. Map of deforested and nondeforested areas over the tropics.
Fig. S6. The 2017 anomalies in remote sensing indices and climate variables.
Fig. S7. Anomalies in the P – ET deficit (mm) and in AGC stocks considering different maps of drylands and humid areas.
Fig. S8. Map of the uncertainty value associated with the recovery date.
Table S1. Land sink (Pg C) and land sink recovery (Pg C) computed from model inversion over the tropics.
Table S2. Fitted parameters (*a*, *b*, *c*, and *d*) in Eq. 1 in the Supplementary Materials for the relationship between L-VOD in 2011 and AGC.

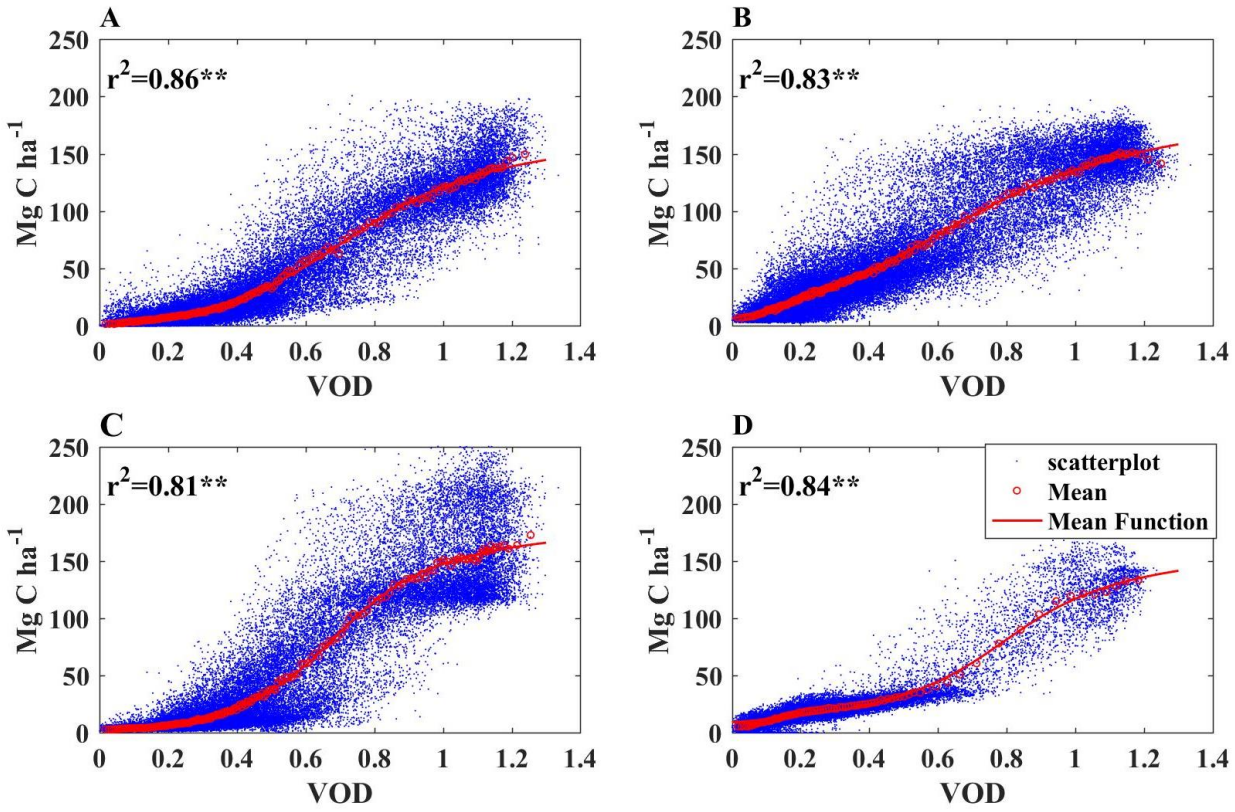

Fig. S1. Scatterplots between yearly mean L-VOD in 2011 and benchmark AGC density maps. The AGC (Mg C ha^{-1}) maps in (**A**, **B**, **C**) are based on the Saatchi, Baccini and Avitabile data sets over the tropics and the map in (**D**) is based on the Bouvet-Mermoz dataset over tropical Africa. The scatterplots indicate the fitted relationship (red) to the mean VOD and AGC densities. The corresponding fitted parameters are summarized in table S2. Scatter plots for tropical Africa and tropical America (not shown) can be found in the Supplementary information of (*17*).

(** indicates significant correlations at $P < 0.01$).

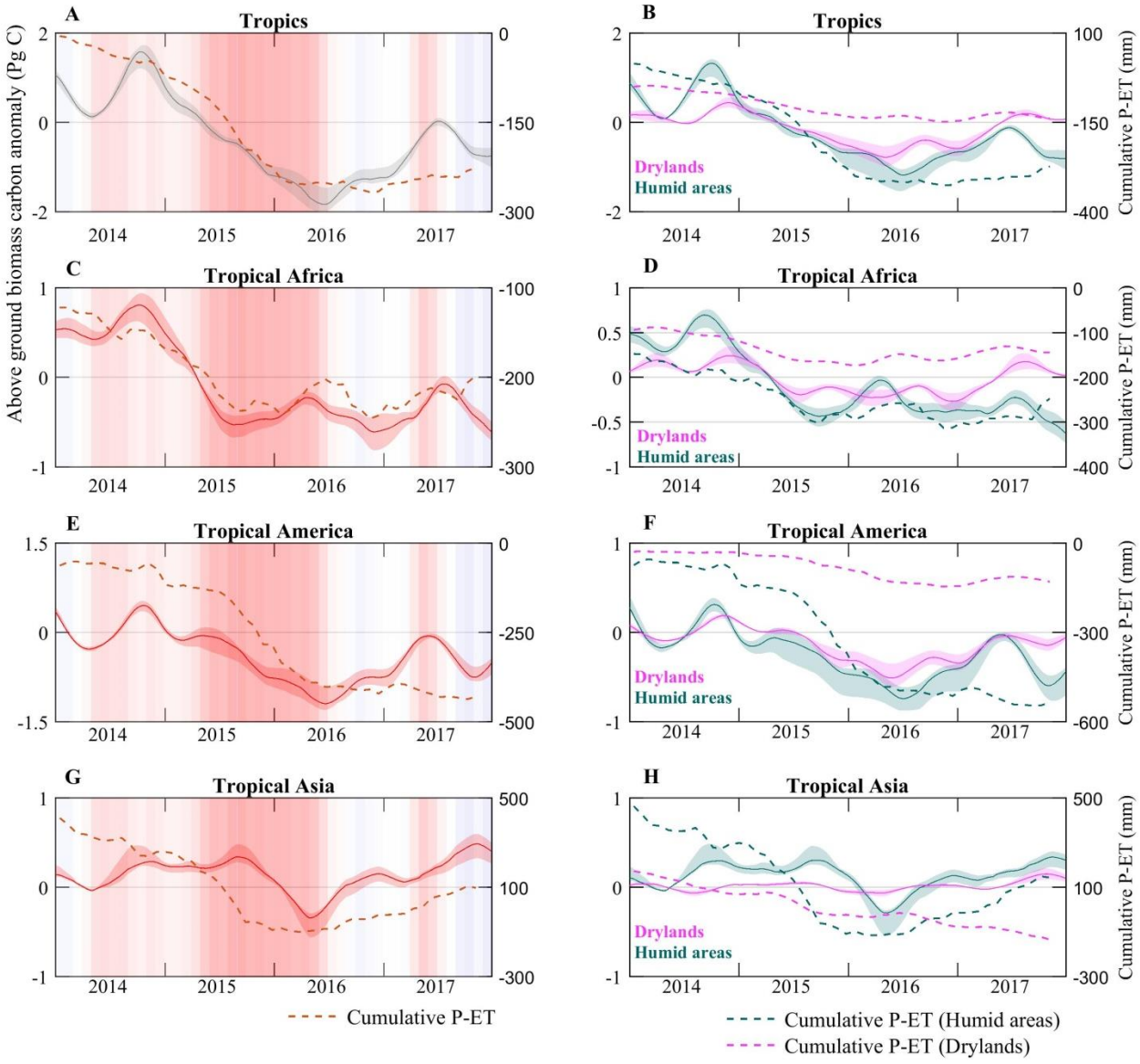

Fig. S2. Anomaly of the P − ET deficit (mm) superimposed on the anomalies of AGC stocks estimated from the L-VOD index in the tropics. (**A**, **C**, **E**, **G**) are time variations in annual AGC over the pan-tropical, tropical Africa, tropical America and tropical Asia regions, respectively. Idem for (**B**, **D**, **F**, **H**), but changes are distinguished for drylands versus humid areas, as defined by the ratio between annual precipitation and potential evapotranspiration (*18*). The AGC anomalies are computed as in Fig. 1 (see Supplementary Materials). The anomalies of the P – ET deficit (mm) are computed at pixel scale, by estimating the time series of P - ET to which we removed its average seasonal cycle.

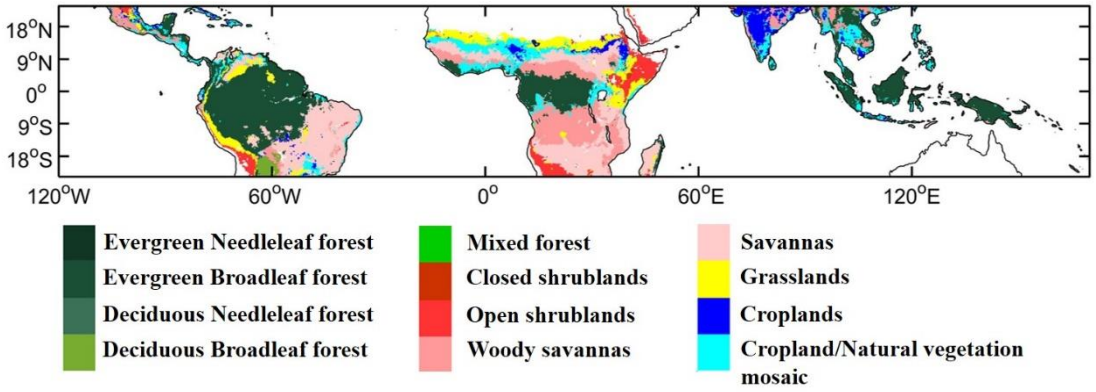

Fig. S3. Biome classes for 2001 to 2010 based on the MODIS IGBP products over the tropics. Classes are aggregated to 25 km by dominant class.

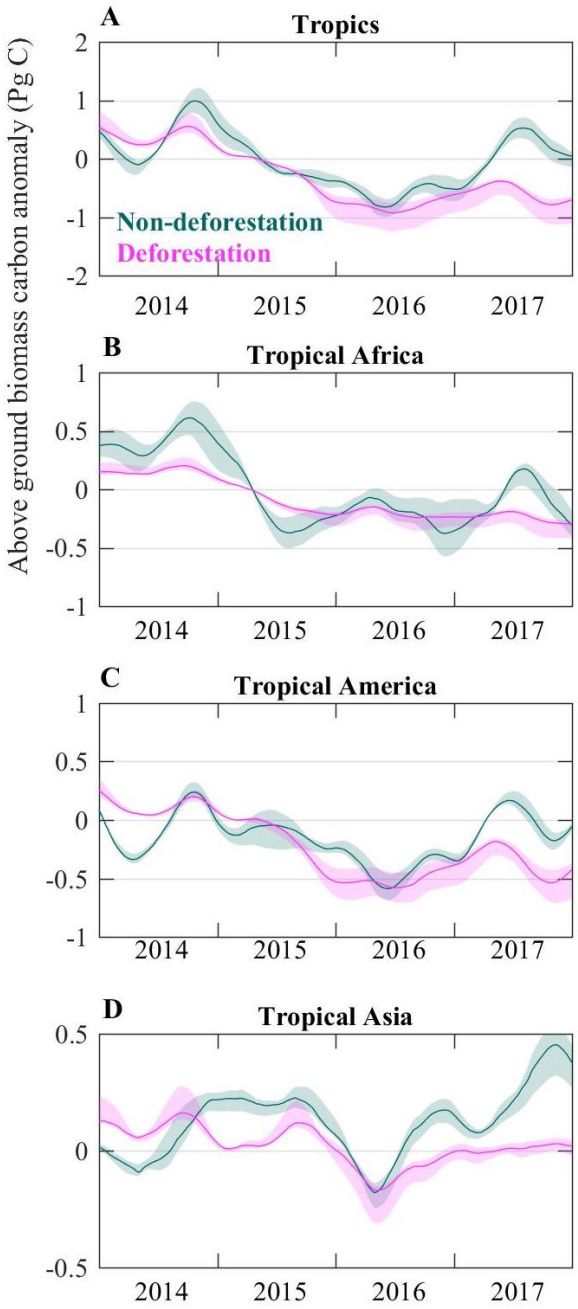

Fig. S4. Anomalies of AGC stocks estimated from the L-VOD index in tropical regions. (**A**, **B**, **C**, **D**) are time variations in annual AGC over the pan-tropical, tropical Africa, tropical America and tropical Asia regions, respectively. AGC changes are separated between deforested and non-deforested areas. The AGC anomalies are computed as in Fig. 1 (see Supplementary Materials). The deforested and non-deforested areas were defined based on the forest area loss map produced by (*20*). Pixels with more than 5% forest losses (covering 16% of the tropics) are considered to correspond to deforested areas (see Supplementary Materials). The map of the deforested and non-deforested areas, as based on that definition, is shown in fig. S5.

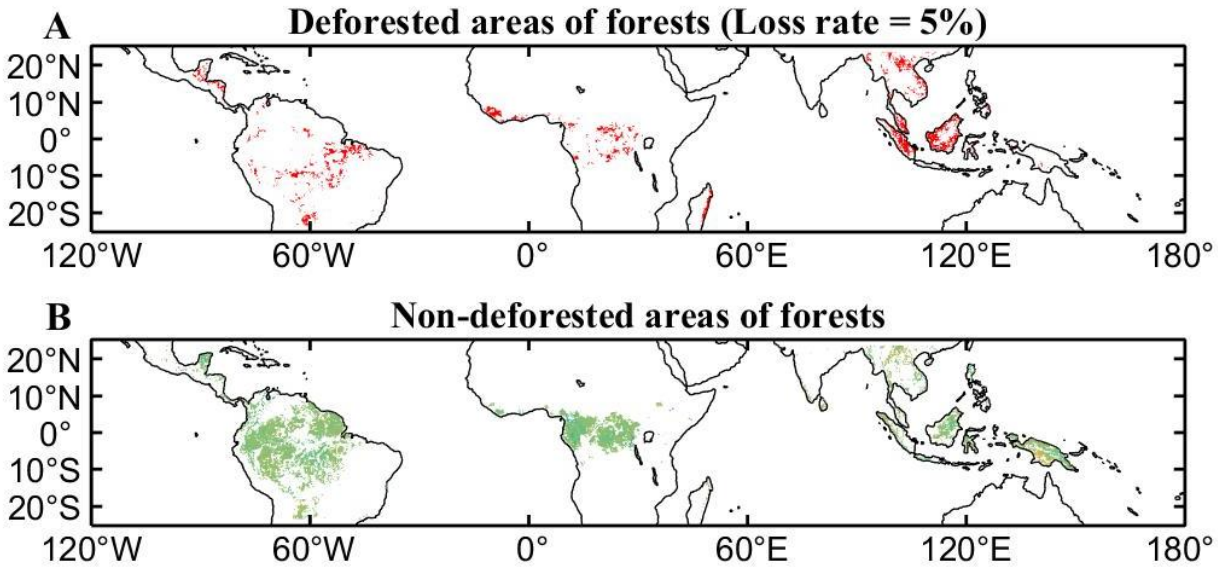

Fig. S5. Map of deforested and nondeforested areas over the tropics. The (**A**) deforested and (**B**) non-deforested areas were defined based on the forest area loss map produced by (*20*). Pixels with more than 5% forest losses (covering 16% of the tropics) are considered to correspond to deforested areas over 2014-2017 (see Supplementary Materials).

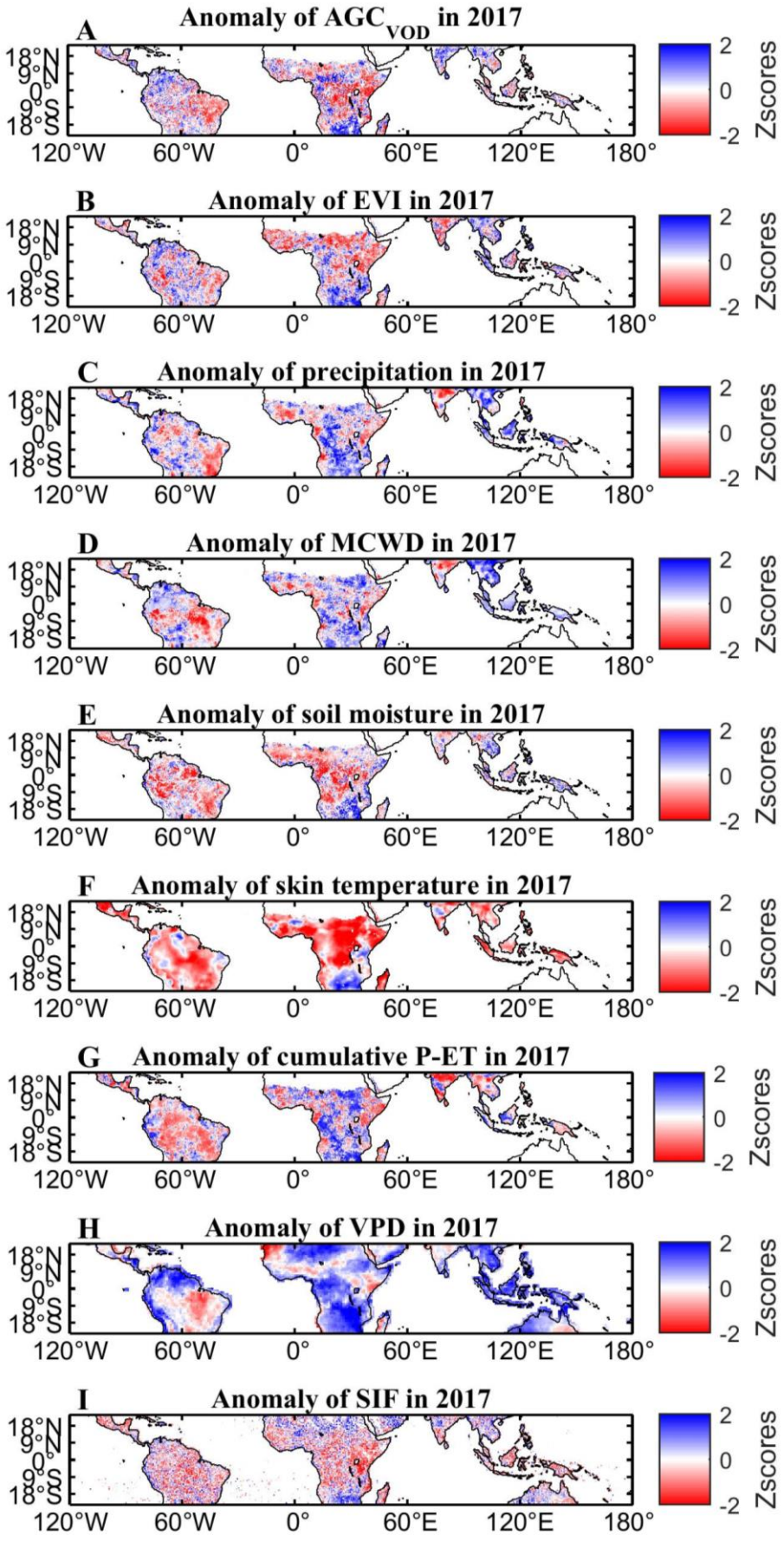
A
Anomaly of AGC$_{VOD}$ in 2017
B
Anomaly of EVI in 2017
C
Anomaly of precipitation in 2017
D
Anomaly of MCWD in 2017
E
Anomaly of soil moisture in 2017
F
Anomaly of skin temperature in 2017
G
Anomaly of cumulative P-ET in 2017
H
Anomaly of VPD in 2017
I
Anomaly of SIF in 2017
18°N
9°N
0°
9°S
18°S
120°W
60°W
0°
60°E
120°E
180°
2
0
-2
Zscores

Fig. S6. The 2017 anomalies in remote sensing indices and climate variables. Anomalies in (**A**) L-VOD inferred aboveground vegetation carbon (AGC_{VOD}), (**B**) enhanced vegetation index (EVI), (**C**) precipitation (**D**) maximum climatological water deficit (MCWD) (**E**) surface soil moisture (SM) (**F**) land surface temperature (**G**) cumulative water balance estimated as the cumulative P –ET value (mm) (**H**) vapor pressure deficit (VPD) (**I**) solar-induced chlorophyll fluorescence (SIF). Yearly anomalies were calculated using the z score: (value − mean)/standard deviation.

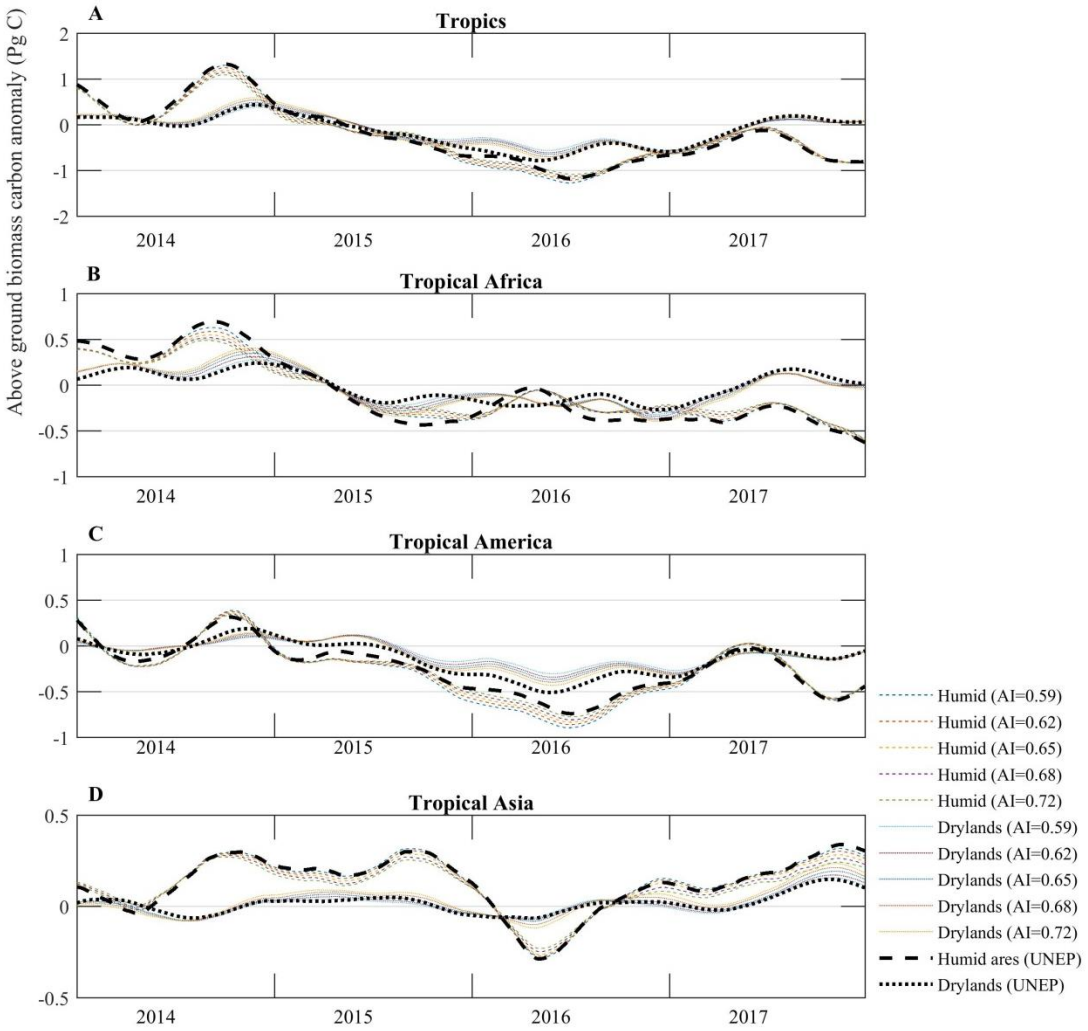

Fig. S7. Anomalies in the P − ET deficit (mm) and in AGC stocks considering different maps of drylands and humid areas. (**A**, **B**, **C**, **D**) correspond to (**B**, **D**, **F**, **H**) in fig. S2. We considered the UNEP map (*19*) and the GAI map (*35*) using different threshold values for the global aridity index GAI: drylands are defined as regions with a GAI index lower than 0.59, 0.62, 0.65, 0.68, and 0.72.

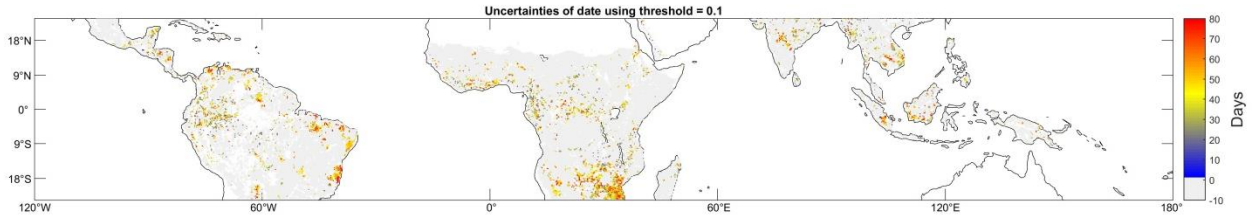

Fig. S8. Map of the uncertainty value associated with the recovery date. The uncertainty value corresponds to a range of days surrounding the date of recovery and is defined as described in Supplementary Methods

Table S1. Land sink (Pg C) and land sink recovery (Pg C) computed from model inversion over the tropics. The land sink recovery was computed as the average of the land sink over 2017 minus that over 2015-2016 (as in Table 1: positive sign for a carbon land surface sink, negative sign for a carbon land surface source). Five observation-based datasets of net land-atmosphere surface fluxes were used: the Copernicus Atmosphere Monitoring Service (CAMS) atmospheric inversion version 16r1 (*48*), the Jena CarboScope inversion versions s76_v4.1 and s85 (*49*), JAMSTEC (*50*) and CarbonTracker Europe (CTE) (*51*).

Model/ Year	CAMS	CarboScope_s76	CarboScope_s85	JAMSTEC	CTE
Sink 2014	+0.19	+0.69	+0.71	+0.37	+1.08
Sink 2015	-0.92	-0.15	-0.44	-0.45	+0.08
Sink 2016	-0.68	-0.33	-0.80	-0.71	-0.08
Sink 2017	+1.13	+0.57	+0.42	+0.19	-0.09
Land sink Recovery	+1,92	0,81	1,04	0,77	-0,08

Table S2. Fitted parameters (*a*, *b*, *c*, and *d*) in Eq. 1 in the Supplementary Materials for the relationship between L-VOD in 2011 and AGC. Values are given for the four benchmark maps for three tropical areas (Africa, America and the entire tropical region) (*17*).

Abbreviation	AGC	Region	*a*	*b*	*c*	*d*	r^2	RMSE (Mg ha^{-1})
$P_{African\ Saatchi}$	Saatchi	Tropical Africa	158.858	4.228	0.673	0.912	0.999**	1.24
$P_{american\ Saatchi}$	Saatchi	Tropical America	215.548	2.090	0.738	-7.390	0.997**	2.56
$P_{tropical\ Saatchi}$	Saatchi	Tropics	183.635	2.822	0.718	-1.117	0.997**	2.25
$P_{African\ Baccini}$	Baccini	Tropical Africa	251.969	1.661	0.760	4.838	0.998**	1.89
$P_{america\ Baccini}$	Baccini	Tropical America	162.904	2.812	0.614	20.800	0.997**	2.50
$P_{tropical\ Baccini}$	Baccini	Tropics	203.168	1.964	0.586	6.458	0.997**	2.41
$P_{African\ Avitabile}$	Avitabile	Tropical Africa	204.163	7.173	0.720	0.962	0.998**	1.98
$P_{American\ Avitabile}$	Avitabile	Tropical America	200.663	2.709	0.666	-4.644	0.999**	1.98
$P_{tropical\ Avitabile}$	Avitabile	Tropics	195.103	3.965	0.685	-0.990	0.999**	2.03
$P_{African\ Bouvet}$	Bouvet-Mermoz	Tropical Africa	185.119	2.707	0.823	5.600	0.990**	3.12

** indicates significant correlations at $P < 0.01$.